

Lawrence Berkeley National Laboratory

LBL Publications

Title

Quantifying Subsurface Flow and Solute Transport in a Snowmelt-Recharged Hillslope With Multiyear Water Balance

Permalink

<https://escholarship.org/uc/item/58m5w5wb>

Journal

Water Resources Research, 58(12)

ISSN

0043-1397

Authors

Tokunaga, Tetsu K

Tran, Anh Phuong

Wan, Jiamin

et al.

Publication Date

2022-12-01

DOI

10.1029/2022wr032902

Copyright Information

This work is made available under the terms of a Creative Commons Attribution License, available at <https://creativecommons.org/licenses/by/4.0/>

Peer reviewed

Water Resources Research



RESEARCH ARTICLE

10.1029/2022WR032902

Quantifying Subsurface Flow and Solute Transport in a Snowmelt-Recharged Hillslope With Multiyear Water Balance

Key Points:

- Large contrasts in annual precipitation are essential for constraining hydraulic conductivity profiles estimated by transmissivity feedback
- Flow and transport during snowmelt occur predominantly within shallow depths because water table rise amplifies transmissivities
- A framework is presented for estimating subsurface flow and transport on hillslopes based on sparsely distributed measurements

Correspondence to:

T. K. Tokunaga,
tktokunaga@lbl.gov

Citation:

Tokunaga, T. K., Tran, A. P., Wan, J., Dong, W., Newman, A. W., Beutler, C. A., et al. (2022). Quantifying subsurface flow and solute transport in a snowmelt-recharged hillslope with multiyear water balance. *Water Resources Research*, 58, e2022WR032902. <https://doi.org/10.1029/2022WR032902>

Received 27 MAY 2022

Accepted 1 DEC 2022

Corrected 20 MAR 2023

This article was corrected on 20 MAR 2023. See the end of the full text for details.

Author Contributions:

Conceptualization: Tetsu K. Tokunaga

Data curation: Tetsu K. Tokunaga, Jiamin Wan

Formal analysis: Tetsu K. Tokunaga, Anh Phuong Tran, Wenming Dong

Funding acquisition: Kenneth H. Williams

Investigation: Tetsu K. Tokunaga, Anh Phuong Tran, Jiamin Wan, Alexander W. Newman, Curtis A. Beutler, Wendy Brown, Amanda N. Henderson, Kenneth H. Williams

© 2022. The Authors.

This is an open access article under the terms of the [Creative Commons Attribution-NonCommercial-NoDerivs License](https://creativecommons.org/licenses/by-nc-nd/4.0/), which permits use and distribution in any medium, provided the original work is properly cited, the use is non-commercial and no modifications or adaptations are made.

Tetsu K. Tokunaga¹ , Anh Phuong Tran², Jiamin Wan¹ , Wenming Dong¹ , Alexander W. Newman³ , Curtis A. Beutler³ , Wendy Brown³ , Amanda N. Henderson³ , and Kenneth H. Williams¹ 

¹Lawrence Berkeley National Laboratory, Berkeley, CA, USA, ²Water Resources Institute, Hanoi, Vietnam, ³Rocky Mountain Biological Laboratory, Gothic, CO, USA

Abstract Quantifying flow and transport from hillslopes is vital for understanding water quantity and quality in rivers, but remains obscure because of limited subsurface measurements. Using measured hydraulic conductivity K profiles and water balance over a single year to calibrate a transmissivity feedback model for a hillslope in the East River watershed (Colorado) proved unsatisfactory for predicting flow over the subsequent years. Well-constrained field-scale K were obtained by optimizing subsurface flux predictions over years having large differences in recharge, and by including estimates of interannual transfer of excess snowmelt recharge. Water and solute exports during high snowmelt recharge occur predominantly via shallow groundwater flow through weathered rock and soil because of their enlarged transmissivities under saturated conditions. Conversely, these shallow pathways are less active in snow drought years when the water table remains deeper within the weathering zone. Hillslope soil water monitoring showed that rainfall does not infiltrate deeply during summer and fall months, and revealed water losses consistent with model ET predictions. By combining water table-dependent fluxes with pore water chemistry in different zones, time-dependent rates of solute exports become predictable. As an example, calibrated K were combined with dissolved nitrogen concentrations in pore waters to show the snowmelt-dependence of reactive nitrogen exported from the hillslope, further supporting the recent finding that the weathering zone is the dominant source of reactive nitrogen at this site. Subsurface export predictions can now be obtained for wide ranges of recharge based on measurements of water table elevation and profiles of pore water chemistry.

1. Introduction

Understanding subsurface flow and transport in hillslopes is needed for predicting a number of important processes including exports into riparian zones and surface waters (Jencso et al., 2010; McGuire & McDonnell, 2010; Penna et al., 2015; Spencer et al., 2021), bedrock weathering (Ameli et al., 2017; Anderson & Dietrich, 2001; Wan et al., 2019), and slope stability (Arnone et al., 2011; Godt et al., 2008; Uchida et al., 2001). Because of the stratified nature of solute concentration profiles in the subsurface, distributions of water fluxes among different zones need to be understood for predicting solute exports. However, the heterogeneous subsurface hydraulic properties that modulate flow can only be sparsely characterized, and local measurements in soil and shallow saprolite are known to severely underestimate values of hydraulic conductivity, K , needed to represent flow at the hillslope scale (Brooks et al., 2004; Di Prima et al., 2018; Glaser et al., 2016, 2019; Uchida et al., 2001; Weiler et al., 2005; Wilson et al., 2016). Characterization of spatially complex aqueous geochemistry of the hillslope subsurface via pore water sampling is also challenging (Boggs & Adams, 1992; Weihermuller et al., 2006), yet needed in combination with water fluxes for determining transport of solutes. Thus, simplifying approximations are needed in order to predict hillslope behavior based on sparse local measurements. In hillslopes where values of K increase toward to the soil surface, the transmissivity feedback model provides a practical simplification for the problem of groundwater flow responses to recharge events (Bishop et al., 2004; Kendall et al., 1999; Rodhe, 1989). The transmissivity feedback model describes downslope flow responses to rainfall or snowmelt recharge through accommodating new recharge within a rising water table, that is, within a thicker and hence more transmissive saturated zone.

When combined with pore water chemistry, a prominent advantage of the transmissivity feedback framework is that it provides insights into the time- and depth-dependent transport of solutes in hillslope pore waters, thereby directly yielding relations between solute concentrations C and rates of hillslope discharge Q . Catchment- and

Methodology: Tetsu K. Tokunaga, Anh Phuong Tran, Jiamin Wan

Project Administration: Kenneth H. Williams

Resources: Tetsu K. Tokunaga, Jiamin Wan, Kenneth H. Williams

Software: Tetsu K. Tokunaga, Anh Phuong Tran

Validation: Tetsu K. Tokunaga

Writing – original draft: Tetsu K. Tokunaga

Writing – review & editing: Tetsu K. Tokunaga

watershed-scale $C-Q$ relations are commonly obtained from measurements in rivers, yet such integrated results lack insights into relative contributions from distinct strata. Models of $C-Q$ relations for river waters sometimes assume that overland flow occurs, and that the dilute endmember water quality is equivalent to that of the precipitation (snow or rainfall) deposited on the watershed (Chanat et al., 2002; Evans & Davies, 1998). More general two-component $C-Q$ models implicitly include infiltrated rainfall and snowmelt fluxes through the shallow surface as part of the runoff end-member (Miller et al., 2014; Pinder & Jones, 1969). An important aspect of the water balance on this hillslope is that although the water table can rise from the weathering zone into the soil during snowmelt, overland flow has never been detected in more than 5 years of field observations. Lack of overland flow simplifies and constrains the flow domain to remain within the subsurface, and at our hillslope the most dilute endmember in subsurface $C-Q$ consists of snowmelt flowing downslope within the soil while the water table is at its highest level.

We recently applied an estimate of total subsurface flow over the course of 1 year to help constrain transmissivity feedback calculations for a hillslope in the Rocky Mountains of Colorado, idealized as a four-layer system consisting of fractured bedrock, weathering zone, subsoil, and surface soil, and introduced an approach for predicting subsurface concentration-discharge ($C-Q$) relations (Tokunaga et al., 2019). This methodology provided a framework for quantifying chemical weathering of bedrock (Wan et al., 2019), and for explaining the importance of bedrock weathering for nitrogen (N) exports to the hydrosphere and atmosphere (Wan et al., 2021). In those recent applications, $P-ET$, the difference between annual precipitation P and calculated annual evapotranspiration ET , for a single year (from 12-1-2016 to 11-30-2017) was equated to the net subsurface flow for that time interval, and transmissivities were adjusted within different layers in order to meet this water mass balance requirement. The measured K profile could be made compatible with $P-ET$ by adjusting the thickness of the bedrock layer (i.e., adjusting the depth to impermeable bedrock). Because K values obtained from flow measurements in auger holes and boreholes poorly represent field-scale K , combinations of K values varying by orders of magnitude were able to match the required net subsurface flow over the year, leaving high levels of uncertainty for flow and transport within each layer. Although the chemistry of pore waters varies among the different zones, average values within each zone vary by less than an order of magnitude. Therefore, the uncertainties in K largely dictate the uncertainties in overall solute exports from the hillslope, and point to the need for improving estimates of flow.

A fundamental shortcoming of the procedure used in our earlier work (Tokunaga et al., 2019) was that subsurface flow based on $P-ET$ over only a single year was used to estimate hillslope-scale hydraulic properties, resulting in poor constraints on K values as well as on distributions of fluxes among all layers. These shortcomings were magnified by the fact that calibrations were done using a water year that received nearly the highest recorded precipitation. In order to understand climate-dependent trends relating reduced flow, and changes in water quality of rivers and lakes, accurate representations of hillslope and watershed responses under lower recharge are needed (Rogora et al., 2020; Todd et al., 2012). Given the potential increased frequency of snow drought years under changing climate (Dierauer et al., 2019; Marshall et al., 2019; Shrestha et al., 2021), improved estimates of hillslope K profiles are clearly needed to represent subsurface flow over widely ranging amounts of recharge. Given the dependence of subsurface flow on water exchanges with the atmosphere, the representativeness of P and calculated ET also warrant further examination.

While variations in $P-ET$ over multiple years are reflected in year-to-year differences in subsurface discharge, this strategy remains an approximation because of interannual variability in subsurface storage (Niu et al., 2017; Rice & Emanuel, 2019; Wang, 2012). From the water balance equation, total annual discharge from the hillslope is given by

$$Q_a = P - ET - \Delta S \quad (1)$$

and storage changes, ΔS , are generally needed, especially when considering multiple water years with significantly different $P-ET$. Because the fractured bedrock remained saturated throughout the 5 years of our study, ΔS represents saturation changes soil and the weathering zone. It should be noted that annual intervals here are based on water years beginning on October 1.

Previously obtained evidence that ET was sufficiently high for preventing groundwater recharge from summer monsoon rains (Tokunaga et al., 2019) suggests that variations in snowmelt recharge largely influence interannual differences in subsurface storage at our hillslope. Indeed, given large variations in snowpack accumulation among different water years, portions of recharge from high snowpack years can contribute to flow in the subsequent

year. Thus, a second shortcoming in our previous approach was that “excess” snowmelt from 1 year was not allowed to carry over into the following year's subsurface flow. In this work, ΔS is not explicitly tracked, but instead is approximated through transferring the portion of winter snow precipitation that exceeds a threshold level P_{isp} to the following year's precipitation. In high snowpack years, the effective annual precipitation P_e equals annual P minus the excess snow precipitation. Otherwise, P_e equals annual P plus any carryover from the previous year. With this simplification, the water balance is effectively closed as

$$Q_a = P_e - ET \quad (2)$$

Uncertainty in this approach will be quantified through the minimized root mean square differences (rmsd) between Q_a and $P_e - ET$ over 5 years that included a near-record high snowpack and snow droughts.

Poorly constrained K profiles for the hillslope also diminish predictive capabilities with respect to solute exports into the floodplain and river receiving subsurface fluxes because transport produces flow-weighted concentrations, and concentrations of dissolved components vary with depth. For example, base cations (Ca^{2+} , Mg^{2+} , Na^+ , K^+) tend to be most concentrated in the weathering zone, while soluble reduced species (e.g., Fe^{2+}) are released in pore waters of deeper strata (Wan et al., 2019). Conversely, dissolved organic carbon (DOC) concentrations are highest within surficial soil horizons (Michalzik et al., 2001) that also have the highest K , such that DOC export is greatest when snowmelt raises the water table up into this most transmissive shallow zone (Tokunaga et al., 2019).

In the present work, the water balanced transmissivity feedback approach is calibrated over 5 years having wide ranges in annual P , with an approach that assumes negligible storage changes while transferring the portion of snowpack P exceeding a threshold level to ΔS for contribution to the following year's subsurface flow. It is emphasized that increasing the number of years included in the calibration cannot significantly improve constraints on hydraulic properties when only small interannual variations in P and ET occur, because little variability would result in annual recharge hydrographs. However, multi-year calibration becomes advantageous when they include years with and without sufficiently high recharge to raise the water table into the soil to activate rapid, shallow flow. The advantage arises with these conditions because a suitable transmissivity profile must be found to satisfy flow in years when the very high K soil zone does and does not participate in discharge. The resulting K profile combined with water table data closely reproduces recharge responses from both high snowpack and snow drought years. Representation of both P and ET are improved through using data from a weather station closer to the hillslope. In addition, independent analyses of soil water losses during summer and fall were performed that provide support for model calculations of ET losses.

The ability to accommodate large variations in annual recharge with transmissivity feedback discharge predictions is important in view of highly variable annual snowfall (Cayan, 1996; Lute & Abatzoglou, 2014; Woodhouse & Pederson, 2018; Xiao et al., 2018), and the previously noted occurrence of snow drought years. These considerations also lead to improved estimates of the partitioning of downslope flow along the different zones (surface soil, subsoil, weathering zone, and bedrock) throughout each water year. Improvements to flux calculations resulting from multiyear water balances and more representative weather data also increase the reliability of predictions for subsurface solute exports, illustrated here for export of dissolved nitrogen from the hillslope.

2. Materials and Methods

Here, an overview of the hillslope site is provided, followed by descriptions of the weather-based annual water balance approach, water table and hydraulic gradient monitoring, calculations of hydraulic properties and flow, pore water quality measurements, and the soil water mass balance approach for determining ET during summer and fall. The weather data and calculated ET are presented here because they provide the basis for the subsurface flow analyses. Furthermore details of the hillslope hydrologic characterization were presented previously (Tokunaga et al., 2019), and are summarized below.

2.1. Site Description and Instrumentation

This meadows-vegetated hillslope in the Colorado Rocky Mountains (USA) is situated on a northeast facing slope (centered at 38.9198° , -106.9493°), and drains into a willows-vegetated floodplain along the upper East

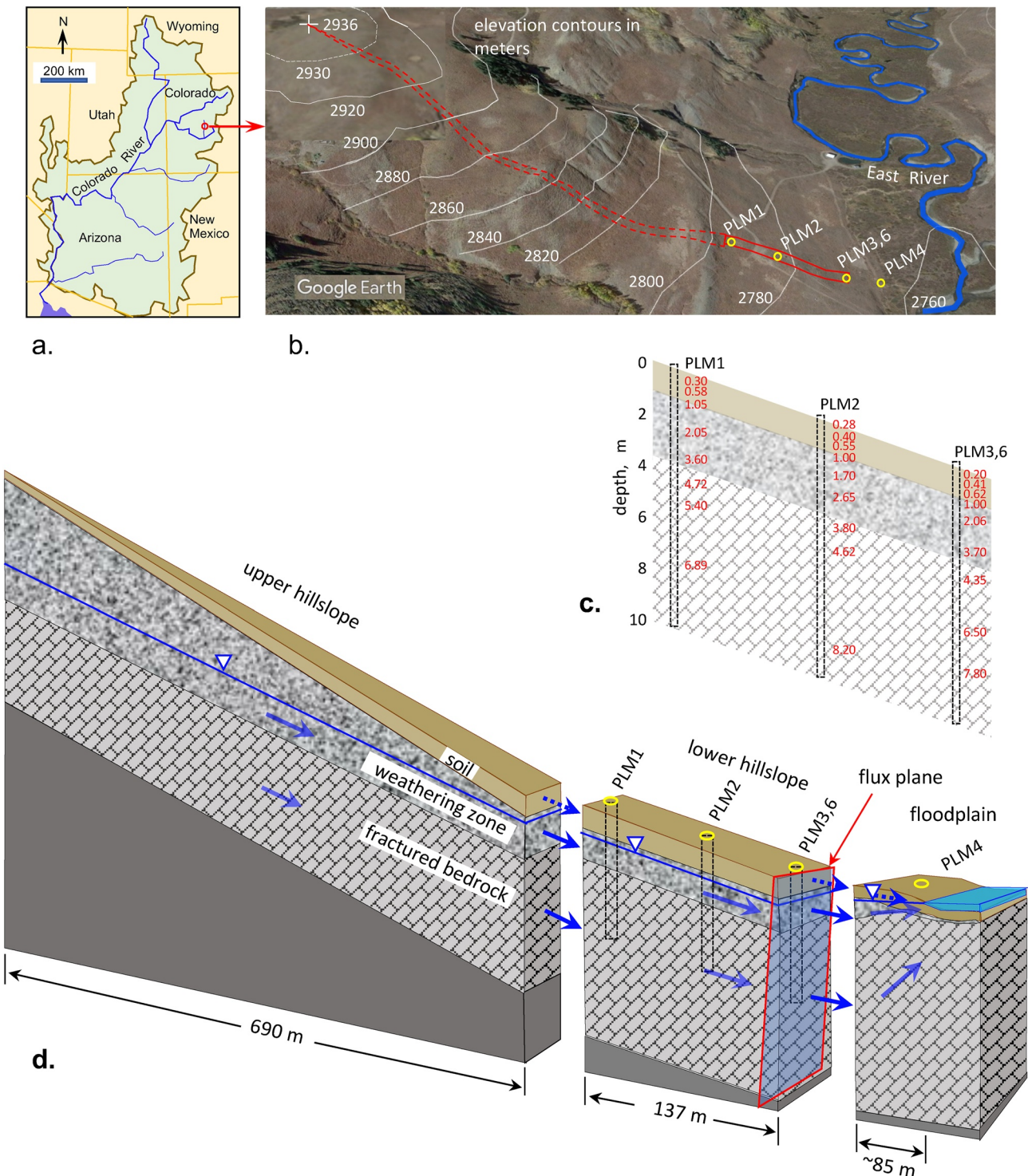


Figure 1. Hillslope site. (a) Location map with outline of Colorado River Basin. (b) Aerial view of site and its relation to the East River. (c) Cross-section through hillslope boreholes showing depths of sensors and pore water samplers in red. (d) Cross-section depiction of upper and lower hillslope sections draining into floodplain and river. The subsurface is subdivided into soil, weathering zone, and fractured bedrock, underlain by effectively impermeable rock at unknown depth.

River (Figure 1a). Topography is used to delineate surface boundaries of the hillslope system. From its local peak (2,936 m elevation), the nearly 1 km long drainage transect consists of upper and lower hillslope segments that drain into a floodplain of the East River. The East River flows into the Gunnison River, a major tributary of the

Colorado River. The upper hillslope segment is not monitored, but provides about 72% of the total subsurface flow exiting the lower transect based on its topography and horizontally projected area estimated by an isosceles triangle with 690 m sides and a base of 1.0 m at the interface with the lower hillslope segment (Figure 1b). Subsurface flow is analyzed along the lower segment of the hillslope, varying in elevation from 2,760 to 2,787 m over a distance of 137 m (Figure 1b). Although topography is useful for estimating lateral flow boundaries (Freeze, 1972; Hubbert, 1940; Toth, 1963), it should be noted that subsurface flow diversion along zones with large differences in K (not detected here) can drive flow across boundaries inferred from surface elevations (Freeze & Witherspoon, 1967; Gleeson & Manning, 2008).

The lower hillslope subsurface consists of about 1.0 m thick loam to silt loam soils, overlying about a 2.6 m thick zone of weathering shale, overlying fractured Mancos Shale bedrock. Measurements of K were obtained from steady-state flow in augered boreholes and transient water level recovery in piezometers (Tokunaga et al., 2019), yielding average values for the 0.5 m thick surface soil, 0.5 m subsoil, weathering zone, and fractured bedrock of $K_{s1} = 9.7 \times 10^{-6}$, $k_{s2} = 7.9 \times 10^{-6}$, $K_{wz} = 1.1 \times 10^{-5}$, and $K_{bf} = 1.7 \times 10^{-7} \text{ m s}^{-1}$, respectively. These K values and the transmissivity of the bedrock are adjusted later to best match annual subsurface fluxes predicted from multi-year $P-ET$. Monitoring of the subsurface was conducted at three stations (PLM1, PLM2, and PLM3/6 depicted in Figure 1c) along the lower hillslope, with their locations having the advantage of integrating flow and transport from a larger upslope area while groundwater remains within a few meters of the soil surface. Instruments embedded in the bedrock, weathering zone, and soil via 10.0 m deep boreholes included matric potential sensors (Decagon MPS-6), volumetric water content sensors (Decagon 5 TE), and pore water samplers (Soil moisture Equipment 1920FIL06-B02M2). In addition, piezometer pipes installed at PLM1 and PLM6 were instrumented with pressure transducers (AquaTROLL 200) for continuous recording of water table elevations.

2.2. Weather Data, Modeled Evapotranspiration, and Annual Water Balance

Daily air temperature and precipitation data were obtained from the Butte SNOTEL weather station (USDA, 2021), located 3.1 km south of the hillslope. This station is 2.2 km closer to the hillslope than the one at Gothic used in our earlier work, and received on average 22% less annual precipitation over WY2017–WY2021. Correlations between Butte SNOTEL air temperatures and shorter-term air temperature data from station ER-CSMWS (Versteeg & Williams, 2021) located 0.3 km from the hillslope were used to estimate daily average (Figure 2a), minimum, and maximum air temperatures at the hillslope needed for ET calculations. Because precipitation data at ER-CSMWS are incomplete, the Butte SNOTEL station was used for daily P values (Figure 2b) and for calculating daily ET for the hillslope (Figure 2c) with the Community Land Model (CLM) (Oleson et al., 2013; Tran et al., 2019). However, some CLM-predicted winter ET rates were as low as 0 mm day^{-1} in our previous work, and recent evaluations of the CLM4 indicated that representations of sublimation could be improved (Toure et al., 2016, 2018). Therefore, during periods with snow cover, largely within the months of November through April, ET was assigned the average sublimation rate of 0.3 mm day^{-1} obtained from eddy covariance measurements in forest openings at other Colorado Rocky Mountain sites (Sexstone et al., 2016). As described later, CLM predictions for summer and fall ET are checked against soil water balance measurements.

Note that annual P varied by nearly a factor of 2 between WY2017 with its above-average snowpack and the following snow drought WY2018, and that a large difference also occurred for annual P in WY2019 and WY2020 (Figure 2b). Compared to variations in annual P , the calculated annual ET was less variable from year to year (Figure 2c), consistent with findings from many other studies (Fatichi & Ivanov, 2014; Garbrecht et al., 2004; Huntington & Billmire, 2014; Niu et al., 2017). Given relatively low variability in annual ET , magnitudes of annual subsurface flow are expected to be strongly correlated to annual P .

The subsurface hillslope water balance at this site was calculated based on water year cycles that begin on October 1 of the previous calendar year and end on the following September 30. Although subsurface water storage continues to decrease with the gradually declining water table into March, the selection of October 1 has the advantage of initiating each year without the presence of a snowpack. As noted earlier, the annual subsurface flow was previously simply estimated from the difference between measured annual P and annual ET calculated using CLM. However, this approach assumed negligible year-to-year changes in net subsurface water storage, hence omits effects of net water storage increases from melting of above-average snowpack that can contribute to the following year's subsurface flow. Indeed, the approximate nature of using $P-ET$ is evident upon considering WY2018, when this approach yielded -8 mm (Figure 2c), indicative of negative discharge and contrary to

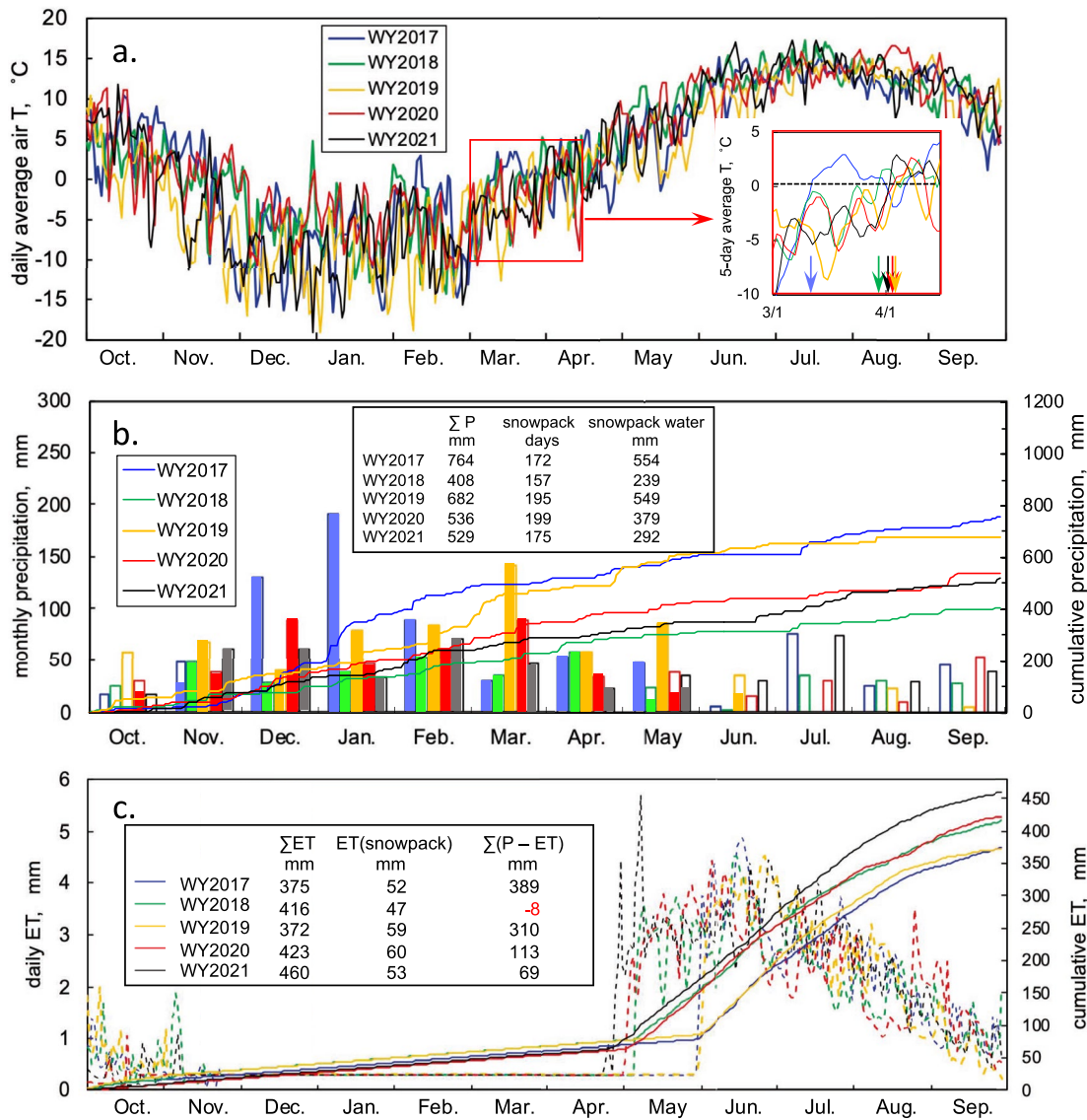


Figure 2. Meteorological conditions at the hillslope site for WY2017–WY2021. (a) Average daily air temperatures. The inset graph shows 5-day running average T during March and April, highlighting the increase above 0°C indicative of snowmelt initiation. Color-coded arrows along the abscissa of the inset graph indicate dates when 5-day average air T began exceeding 0°C. (b) Monthly precipitation (filled = snow, unfilled = rain) and cumulative precipitation. (c) Evapotranspiration calculated with the Community Land Model and an estimated sublimation rate of 0.3 mm day⁻¹ from snow cover.

measured hydraulic gradients that showed continuous discharge from the hillslope throughout the study. Inadequacy of the negligible storage change assumption is further demonstrated through examination of year-to-year variations in water table elevations. Therefore, our recharge-constrained transmissivity feedback approach requires the ability to forward “surplus” snowpack P to effectively contribute to recharge in the following year, as described in Section 2.4.

2.3. Hillslope Water Table Dynamics and Hydraulic Gradients

Continuous monitoring of the water table with pressure transducers at PLM1 and PLM6 showed that the water table only rises during recharge by infiltrating snowmelt, and trends for 5 years are shown in Figure 3a. Reliability of the pressure transducer records was confirmed through occasional comparisons with direct tape measurements of water table depths, and were also shown to be consistent with pressure measurements obtained on pore water samplers (Tokunaga et al., 2019).

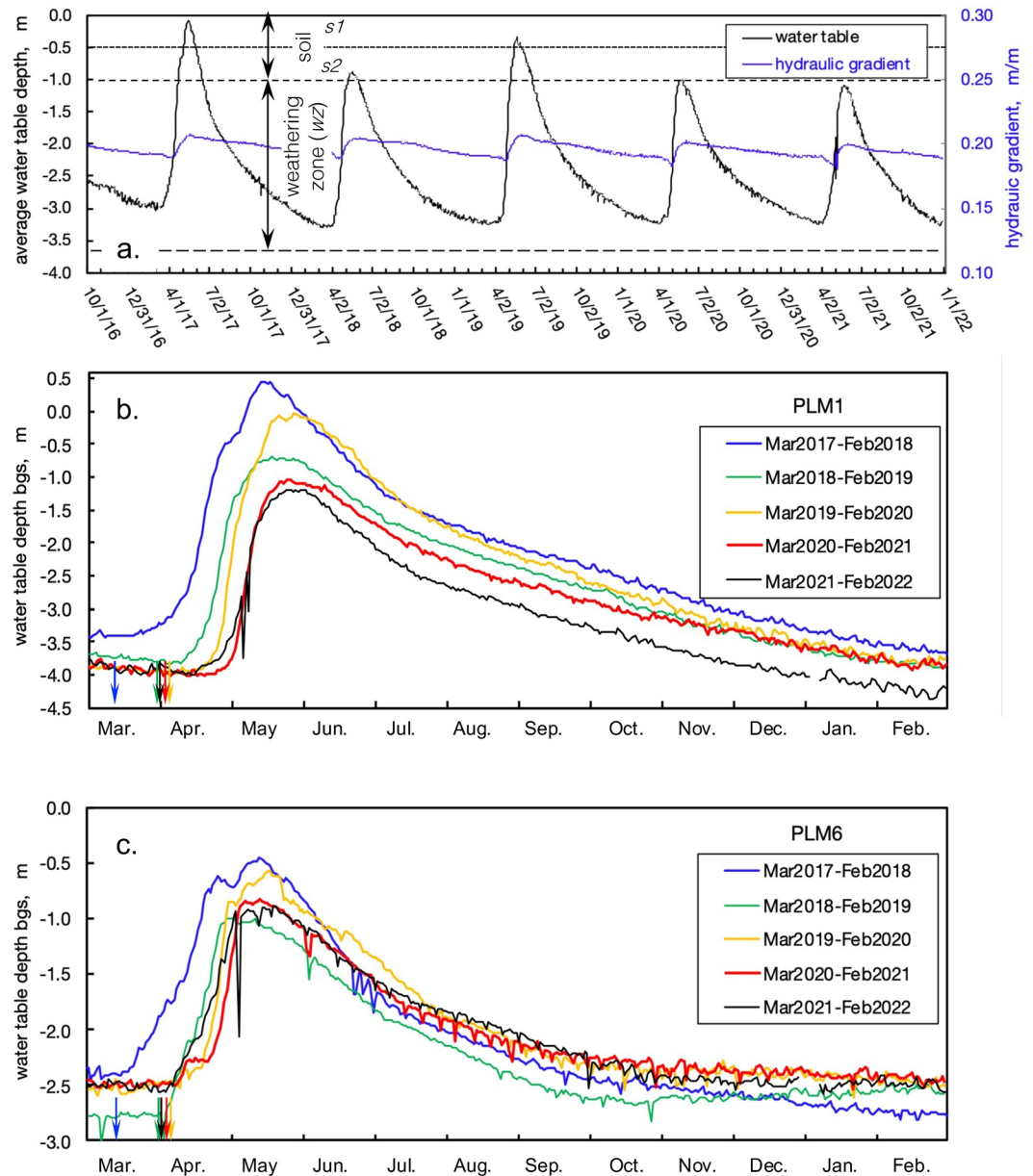


Figure 3. Temporal trends in hillslope water table depth. (a) Average water table depth below the hillslope soil surface and hydraulic gradient between PLM1 and PLM3/6. The water table rises from the weathering zone into the soil zones s2 and s1 when snowmelt recharge is high during WY2017 and WY2019. The trend for the drought WY2018 indicates that residual drainage from the unusually high snowmelt from WY2017 supported water table rise into the soil zone despite low 2018 snowmelt. Annual water table depth variations, showing variations in local behavior among different water years at upslope PLM1 (b) and downslope PLM6 (c), respectively. Color-coded arrows along the abscissa indicate times when 5-day average air T began exceeding 0°C .

Differences between the water table elevations at PLM1 and PLM6 were divided by their separation distance (137 m) to obtain daily values of the hydraulic gradient driving downslope flow, also shown in Figure 3a. The piezometric gradient along the transect remains similar to the overall slope of the soil surface (0.197 m m^{-1}), and ranges between 0.19 and 0.21 m m^{-1} . Based on this behavior, we applied the Dupuit-Forchheimer assumptions that hillslope groundwater flow lines remain parallel, the hydraulic gradient is invariant with depth, and that an impermeable lower boundary is aligned with the parallel flow paths. In addition, Childs' corrections to the Dupuit-Forchheimer approximation for flow along a sloping water table was applied, where groundwater equipotential surfaces are perpendicular to the slope rather than being vertically oriented (Childs, 1971). Thus,

cross-sectional areas for flow are obtained by scaling down the saturated vertical thickness by $\cos\theta$, where θ is the slope between PLM1 and PLM3. For this hillslope with $\theta = 11.2^\circ$, $\cos\theta = 0.98$, a minor reduction. However, on steeper hillslopes, this correction becomes important.

Water level variations from March 1 and February 28(29) are superimposed for the different water years for PLM1 (Figure 3b) and PLM6 (Figure 3c) in order to identify interannual differences. The early occurrence of water table rise at both locations in 2017 relative to the subsequent years is consistent with the early rise of air T shown in Figure 2a. Aside from this T -dependent response in 2017, water table dynamics at PLM6 remained fairly similar between different years because of its location at the base of the hillslope and close proximity to the river. Although WY2017 and WY2019 had above-average snowmelt recharge, water table rise at PLM6 extended only about 0.4 m higher than in other years.

In contrast, the water table dynamics observed at the upslope PLM1 piezometer showed greater sensitivity to magnitudes of snowmelt recharge, with increased peak heights during snowmelt exceeding 1.0 m in WY2017 and WY2019 relative to the other years. Moreover, from Figure 3b it is clear that the magnitude of snowmelt recharge influences later stage baseflow water levels as well, even into the following water year. This further indicates that interannual storage is important and that snowmelt recharge above some high threshold contributes to flow in the following water year. Thus, improvements in the multiyear analyses of subsurface flow will include identification of a threshold level of snowpack P above which snowmelt recharge in a given year is not included in immediate recharge, but instead is carried over to the following year. It should be noted that while the average water table elevation rains above the fractured bedrock throughout the study (Figure 3a), water table recession during the few months prior to snowmelt allows up to about 0.5 m of the uppermost bedrock in the upslope PLM1 location to partially drain (Figure 3b). Nevertheless, because of the unknown yet deep extent of the shale bedrock underlying the hillslope, it will be treated as remaining fully saturated.

2.4. Calculating Hillslope Scale Hydraulic Properties and Flow

In order to calculate downslope flow, the daily average water table elevation along the hillslope is first used to determine the saturated thickness within the weathering zone (1.00–3.60 m depth, w_z) and within the two soil regions (surface 0–0.50 m depth designated s_1 , deeper 0.50–1.00 m depth designated s_2). Because the fractured bedrock remained below the water table during this study, its T was not saturation-dependent. These $\cos\theta$ -scaled thicknesses were multiplied by the saturated K assigned to each layer to obtain their respective transmissivities, T_{s_1} , T_{s_2} , and T_{w_z} . It should be noted that downslope flow parallel to the slope within the soil layer is only effective when the water table resides within the soil, hence T_{s_1} and T_{s_2} are usually zero. Because boreholes were drilled to depths of only 10.0 m below ground surface (bgs), deeper flow cannot be quantified. Therefore, the transmissivity of the permanently saturated fractured bedrock T_{fbr} was among the parameters adjusted to match the estimated annual subsurface flux. Daily subsurface flow was equated to the sum of the four T values times the hydraulic gradient, and these daily flows were summed in order to obtain yearly subsurface flow, Q_a .

Target values for Q_a were equated with P_e-ET , where the effective yearly precipitation P_e is obtained by augmented in P years preceded by heavy snowpack with carryover recharge from that previous year's snowmelt. To conserve overall water mass over multiple years, any snowpack recharge in a given year that exceeded a threshold value was not include in that year's recharge and instead was forwarded to the following water year's precipitation input. The threshold amount of snowpack precipitation, P_{tsp} , above which additional snowmelt is allocated to the following year's subsurface flow is among the adjustable parameters to be optimized. Additional constraints included were that $K_{s_1}, K_{s_2} > K_{w_z} > K_{fbr}$, in keeping with original framework of the transmissivity feedback model. It should be noted that K_{s_1} was not required to be greater than K_{s_2} because studies of soil pipes have provided evidence for hydraulically important buried channels within soils (Uchida et al., 2005). Daily water table-dependent transmissivity-based fluxes for all layers were summed on a yearly basis for WY2017 through WY2021, with variables $K_{s_1}, K_{s_2}, K_{w_z}, T_{fbr}$, and P_{tsp} optimized with the assistance of the Solver regression tool in Microsoft Excel, in order to minimize the rmsd between calculated annual subsurface fluxes Q_a and their associated effective annual P_e-ET . This procedure was implemented with constraints that all variables have finite, positive values, using different initial values for the variables in order to assess suitability of their optimized values. To examine the importance of interannual transfer of snowmelt recharge, the 5-year hydraulic responses were also fit without including P_{tsp} . It is worth noting that while these procedures lead to optimized values of T_{fbr} , values of

b_{fbr} and K_{fbr} remain individually unknown. Indeed, T_{fbr} is a simplifying parameter used in place of depth-dependent bedrock K profiles that can extend kilometers into the subsurface (Kuang & Jiao, 2014; Sanford, 2017).

Because the hydraulic parameters were optimized to yield Q_a that best matched annual P_e-ET , with P_e depending on P , and because annual P and ET are not directly measured at the hillslope, the sensitivity of calculated hydraulic parameters to net water inputs is worth examining. Differences between annual P from the Butte SNOTEL and ET from the CLM are the best available estimates for the hillslope, and will be designated as “reference $P-ET$.” Therefore, deviations of $P-ET$ at the hillslope relative to the reference $P-ET$ were tested to determine their impacts on calculated values of K_{s1} , K_{s2} , K_{w2} , T_{fbr} , and P_{isp} . The weather station at Gothic, Colorado records about 27% greater annual P relative to the Butte SNOTEL, and has more persistent snow than the lower montane hillslope site. Therefore, $\pm 27\%$ deviations from the reference $P-ET$ are unrealistic, and $\pm 15\%$ deviations were applied to examine sensitivity of hydraulic parameters to uncertainties in water exchanges with the atmosphere.

2.5. Dissolved Nitrogen in Pore Water

In order to examine how improving flow calculations impact export of solutes, depth profiles of dissolved nitrogen were obtained by analyses of pore water samples collected from pressure-vacuum samplers. As in our previous study (Wan et al., 2021), dates associated with pore water samples were interpolated between the sampling date and the previous vacuum application date in recognition of the time-dependent inflow of pore waters (Tokunaga, 1992). Based on observations of average sampler response times, the interpolated dates were assigned at one-third the interval between vacuum application and sample collection. For determining TDN, a Shimadzu TOC-VCPH equipped with a total nitrogen module was used. Solute concentrations in each zone were multiplied by their associated transmissivity-dependent flow rates (Section 2.4) to obtain zone-specific solute export rates.

2.6. Summer-Fall ET Measured Through Soil Water Mass Balance

Because the CLM-calculated ET was previously calibrated over coarser scales to encompass variability within the larger upper East River watershed (Tran et al., 2019), independent quantification of ET on the hillslope is useful for assessing the model predictions. While previous soil water potential measurements and predictions from CLM-modeled ET indicated that summer rainfall amounts were insufficient to drive groundwater recharge, actual amounts of ET can be quantified by considering the soil water balance. The soil water balance approach to determining ET is applicable when rainfall and soil moisture measurements are available, especially after soil drainage ceases (Denager et al., 2020; Maule & Chanasyk, 1987; Rana & Katerji, 2000). After drainage cessation, ET is equal to the sum of rainfall and measured net loss of soil water, so that the monitored hillslope can be evaluated like a field-scale weighing lysimeter for determining ET and for evaluating model ET calculations. Although the matric potential ψ at which drainage ceases is dependent on soil texture and can occur at values as low in magnitude (less negative, “wetter”) as -3 to -4 kPa (Assouline & Or, 2014; Maule & Chanasyk, 1987), the traditional “field capacity” ψ of -33 kPa is a more conservative indicator (Colman, 1947), and was used here to determine the volumetric soil water content θ_w profiles at the beginning of summer ET measuring periods. Using this more conservative criterion, the post-snowmelt date on which the deepest matric potential sensor in each soil profile showed that ψ declined to -33 kPa was taken to indicate cessation of soil drainage. Because the specific moisture capacity, $\partial\theta_w/\partial\psi$, decreases with larger magnitude ψ , the -33 kPa criterion has the additional advantage of more stable θ_w values, relative to near-zero ψ that are susceptible to residual drainage of macropores. It is also worth noting that the root mean square errors in the θ_w measured with Decagon 5 TE of about 0.01 (Rosenbaum et al., 2010) are small compared to the differences in water contents among the three hillslope soils (shown later). Among the three hillslope monitoring stations, the drainage cessation condition was generally reached on different days within a given year, and the latest date was selected as the start for cumulative ET calculations. The end of each year's post-snowmelt ET calculation interval was set at 31 October, given common appearance of snow cover during November. Soil and weathering zone samples retrieved by coring rarely contained plant roots below the 1.00 m depth (Wan et al., 2021), therefore ET was calculated from net water loss within the 1.00 m thick soil zone, based on the sum of changes in volumetric water content θ_w from each sensor, weighted by the thickness of each sensor's zone. Boundaries between sensor zones were located midway between adjacent sensor depths, and at the soil surface for the shallowest sensor. Although the soil water balance approach is only applicable at the hillslope over periods of about 4 months out of each year, such intervals are long enough to provide useful comparisons with models.

Net changes in soil water storage at the three monitoring stations were determined through differences between volumetric water content θ_w profiles at cessation of drainage and on October 31 of each year. Most of the θ_w data were obtained with the continuously recording Decagon 5 TE sensors. However, the moisture content sensors at 1.00 and 1.05 m did not provide representative volumetric water contents of deeper hillslope soils because they were embedded in fine sand. For these depths, data from matric potential sensors (Decagon MPS-6) were combined with data on their clay and sand percentages (Tokunaga et al., 2019), and a texture-based model for μ -dependent volumetric soil water content $\theta_w(\mu)$ was used to estimate θ_w (Saxton et al., 1986).

3. Results and Discussion

3.1. Optimized Hillslope Scale Hydraulic Properties and Subsurface Fluxes

To demonstrate improvements obtained from multiyear fitting of the hydraulic properties profile, it is useful to first present our earlier strategy of using measured K profiles and matching annual subsurface flow Q_a to $P-ET$ for a single year by adjusting the bedrock transmissivity T_{fbr} . When transmissivity feedback calculations are done with the average values of measured K within each layer (Section 2.1), T_{fbr} must be set to $1.4 \times 10^{-5} \text{ m}^2 \text{ s}^{-1}$ in order for the calculated annual subsurface discharge Q_a to equal $P-ET$ for WY2017. However, applying these hydraulic properties to the following four years resulted in large overestimates of Q_a relative to $P-ET$ as well as to P_e-ET (Figure 4a). The rmsd between annual $P-ET$ and calculated Q_a for all 5 years was 221 mm, indicating very large overestimated magnitudes of subsurface flow. The sizable errors obtainable with these original parameters becomes even more evident when noting that this rmsd is greater than the calculated 5-year average annual recharge of 175 mm based on either $P-ET$ or P_e-ET .

Optimizing the parameters (K_{s1} , K_{s2} , K_{wz} , T_{fbr} , and P_{tsp}) to match P_e-ET for WY2017 and WY2018 has the advantage of constraining their values to fit a lower recharge year where influences of transmissive flow in the soil layers was minimal. Ranges of K_{s1} , K_{s2} , K_{wz} , T_{fbr} , and P_{tsp} can exactly fit P_e-ET for WY2017 and WY2018 (Figure 4a), with combinations of moderately varying hydraulic properties (Figure 4b). This 2-year optimization yielded a rmsd between Q_a and P_e-ET for the five water years of 71 mm, a substantial improvement over the rmsd obtained with the original parameter set.

By optimizing K and P_{tsp} over years all 5-years, the rmsd between calculated Q_a and P_e-ET was further reduced to 43 mm (Figure 4a). Optimizing the hydraulic properties and threshold snowpack P_{tsp} to all five years (Figure 4b) resulted in values of K_{s1} , K_{s2} , and K_{wz} of 1.43×10^{-4} , 2.68×10^{-4} , and $3.97 \times 10^{-6} \text{ m s}^{-1}$, respectively, $T_{\text{fbr}} = 2.20 \times 10^{-6} \text{ m}^2 \text{ s}^{-1}$, and $P_{\text{tsp}} = 508 \text{ mm}$. The range bars on the two- and 5-year fit K and T in Figure 4b indicate standard deviations for values that are within 1 mm of the rmsd minima for Q_a and P_e-ET . The fit K_{s1} and K_{s2} values are 19- and 34-times greater than their respective auger hole-based field measurements described in our earlier study (Tokunaga et al., 2019), consistent with the previously noted findings that hillslope-scale soil K values are underestimated by local measurements. Conversely, the optimized K_{wz} value is 35% that of the field measurements, the fit T_{fbr} value is only 8% of the estimate obtained in our earlier work (Tokunaga et al., 2019). These improved estimates of hydraulic properties lead to predictions of higher snowmelt recharge responses transmitted downslope via the soil, slight moderation of flow via the weathering zone, and slower baseflow within bedrock. From the optimized threshold snowpack P_{tsp} value of 508 mm and the snowpack water values (inset table within Figures 2b), 46 mm of the P in WY2017 effectively contributes to subsurface flow in WY2018, and 41 mm of the WY2019 P is carried over into WY2020. The occurrence of recharge delay/carryover during these years is consistent with the observed persistence of a shallower water table at PLM1 during these years (Figure 3b).

3.2. Sensitivity of Optimized Parameters to $P-ET$

K and T obtained by matching Q_a to 5 years with $P-ET$ that are 15% greater and 15% less than reference $P-ET$ are shown in Figure 4b for comparison with their values optimized to reference $P-ET$. Systematically higher K and T are obtained for the +15% case in order to accommodate the required increase in subsurface flow. Similarly, lower K and T are obtained for the -15% case in order to transmit reduced subsurface flow. Nevertheless, magnitudes of changes in K and T are not large, indicating that their values for the reference $P-ET$ are suitable. Optimized P_{tsp} of 501 and 522 mm were obtained for the +15% and -15% scenarios, respectively, and are small deviations from the reference value of 508 mm. Next to each of the bars for K and T optimized for the hypothetical higher and lower amounts of recharge is the ratio of its value relative to the corresponding reference case K or T .

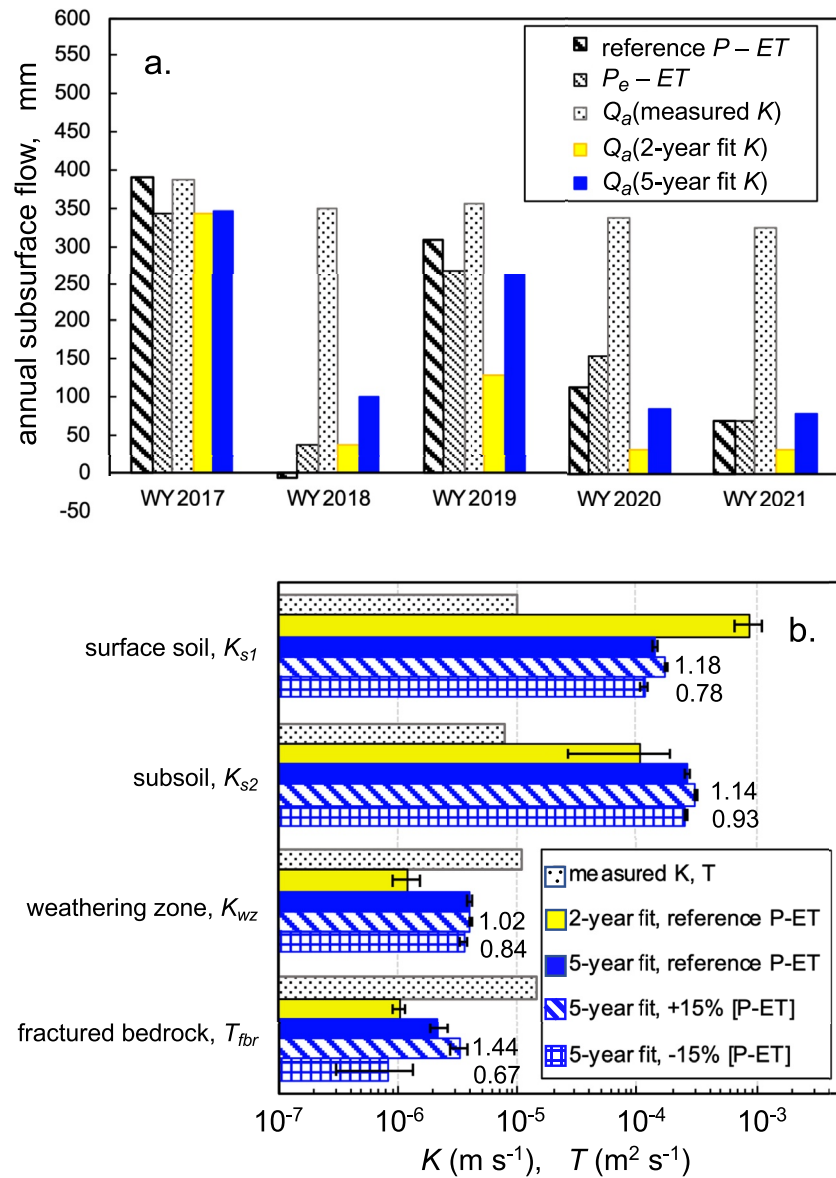


Figure 4. The dependence of calculated annual subsurface flow Q_a on hydraulic properties. (a) Estimates of annual subsurface flow based on $P-ET$, P_e-ET , transmissivity feedback fluxes using measured K and T_{fb} calibrated to yield total subsurface flow in agreement with $P-ET$ for WY2017, and fitting of hydraulic properties to yield fluxes that best match P_e-ET over five years. (b) Comparisons between average local hydraulic properties obtained from measurements in auger holes and piezometers and fit parameter values obtained by matching annual subsurface flow Q_a to P_e-ET . The 2-year fits result in a rmsd between P_e-ET and Q_a of 71 mm when applied to all 5 years. Optimizing hydraulic properties over all 5 years reduces this rmsd to 43 mm. Hydraulic properties consistent with $\pm 15\%$ changes in $P-ET$ are also shown. The uncertainty bars span ranges of K and T that yield rmsd that are within 1 mm of rmsd minima. Ratios of optimized K and T relative to their reference values are shown for the $\pm 15\%$ [$P-ET$] cases.

These ratios deviate from 1.15 for the +15% scenario and from 0.85 for the -15% scenario because of the zone- and time-dependent distribution of fluxes described next.

3.3. Seasonal Dependence of Subsurface Flow, and Responses to Snow Drought

The strong seasonal dependence of subsurface flow on water table depth obtained with the optimized values for hydraulic properties and P_{tsp} is shown in Figure 5. Figure 5a shows the snowmelt-dependent variation in water table depth (left ordinate), and predicted subsurface fluxes transmitted via different zones (right ordinate). In

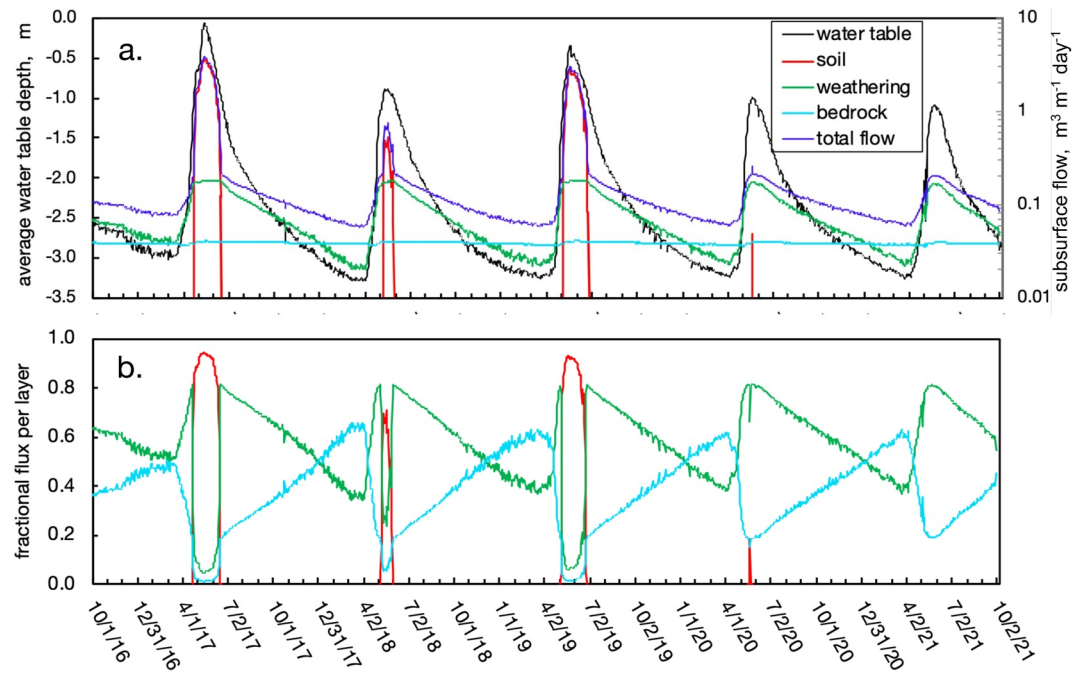


Figure 5. Impacts of annual water table fluctuations on subsurface flow. (a) Annual variations in water table depth and resulting calculated downslope flow along different zones of the hillslope. (b) Time-dependence of fractional contributions of flow along the soil, weathering zone, and fractured bedrock to overall subsurface flow.

this figure, subsurface flow through the transect is expressed in terms of daily volumetric water flow per unit width (normal to the flow direction). Baseflow through the bedrock stays practically steady because it remains fully saturated and the hydraulic gradient only undergoes minor fluctuations during snowmelt events. Flow along the weathering zone fluctuates in response to the continuously varying water table depth that drives continuous variations in its saturated thickness and T_{wz} . Downslope flow along the soil zones is only activated when snowmelt is sufficient to raise the water table from the weathering zone to within 1.0 m of the hillslope surface, and Figure 3a showed that this occurred every year of this study except for the snow droughts of WY2020 and WY2021. Although such periods with high water table elevations are short, they facilitate very high flow rates because of the high K_{s1} and K_{s2} . The importance of transmissive flow within the soil layer during snowmelt is further illustrated in Figure 5b, where subsurface flow in each zone is expressed as a fraction of the daily total subsurface flow. In high snowpack years, over 90% of the snowmelt pulse can be transported along the soil during short periods while the water table resides close to the surface. Outside of periods dominated by spring snowmelt, Figure 5b shows that fractional contributions to subsurface flow in the weathering zone and fractured bedrock annually oscillate, with flow via the bedrock typically becoming dominant during the 2 months prior to snowmelt.

The recharge-dependent patterns shown in Figure 5 point to changes in subsurface flow and transport that can be anticipated from increased frequency of snow drought years. Recall that WY2018 and WY2020 received below-average snowfall, but were preceded by years with above-average snow (Figure 2b) that provided carry-over of storage from WY2017 and WY2019, respectively. In contrast, WY2020 and WY2021 were consecutive snow drought years. As the frequency of snow droughts increases, depletion of subsurface water storage from back-to-back snow drought years may become more common (Alvarez-Garreton et al., 2021). Because such depletion is strongly linked to greater depths of annual water table recession prior to snowmelt recharge, previously continuously water saturated bedrock will become exposed to atmospheric oxygen with greater frequency. Indeed, this phenomenon was demonstrated in water table elevations at PLM1 immediately following snowmelt in WY2021, with water levels declining by more than 0.50 m relative to previous measurements obtained at the same time of the year (Figure 3b). Given the importance of water table elevation on oxidative weathering of shale bedrock (Brantley et al., 2013; Wan et al., 2019; Winnick et al., 2017), climate change-induced alteration of the snowpack in mountainous watersheds can be expected to accelerate bedrock weathering.

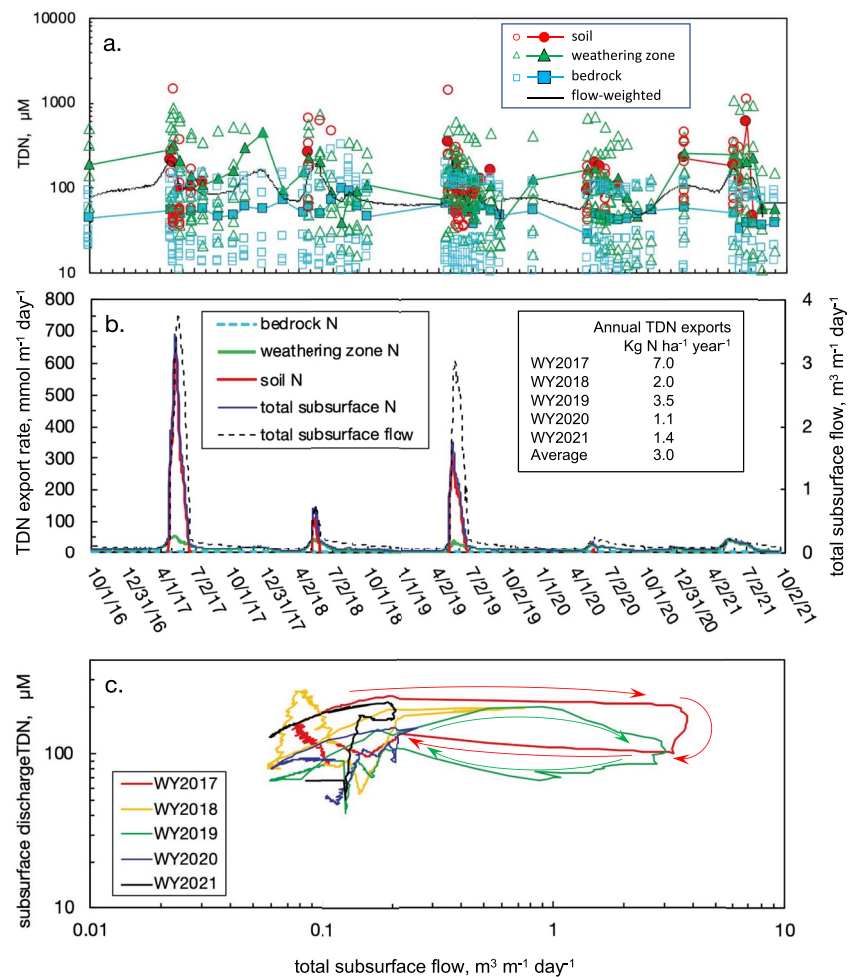


Figure 6. Hillslope subsurface total dissolve nitrogen (TDN) concentrations and transport. (a) Time trends in TDN concentrations in pore waters, (b) calculated TDN export rates along different zones of the hillslope, and (c) subsurface $C-Q$ relations for TDN over five water years.

3.4. Transport of Dissolved Nitrogen

The use of transmissivity feedback for calculating how subsurface flow drives the export of hillslope solutes to the floodplain and river is demonstrated here for total dissolved nitrogen (TDN), consisting primarily of nitrate and ammonium ions. Individual values for measured TDN concentration in pore waters from soil, weathering zone, and bedrock are shown as data points in Figure 6a, along with trendlines through linearly interpolated daily average concentrations in each zone. Concentrations are usually highest in the weathering zone, the source of most of the TDN released during weathering of shale (Wan et al., 2021). Lowest TDN concentrations occur in the bedrock porewaters, consistent with denitrification in reducing waters.

Flow-weighted overall average TDN concentrations in discharge waters were obtained by summing products of daily zone-specific TDN concentrations and their associated fractional fluxes (Figure 5b), and are presented as the black curve in Figure 6a. Multiplying the daily values of pore water concentrations (Figure 6a) by their zone-specific flow rates (Figure 5a), yields the transport rates for TDN within each zone shown in Figure 6b. The trends for TDN export rates show that most of the nitrogen export occurs during two-month periods of snowmelt, accounting for 82% of the annual export during WY 2017, and averaging 57% of TDN exports for all five years. Although nitrogen concentrations were on average greatest in the weathering zone, TDN exports occurred primarily via the soil when snowmelt was large enough to support very high flow rates when the shallow water table rose into the soil. Based on the improved estimates of subsurface fluxes, the overall TDN export rate amounts to 3.0 kg N ha⁻¹ y⁻¹, a value that is lower than that previously reported 10.6 kg N ha⁻¹ y⁻¹ (Wan

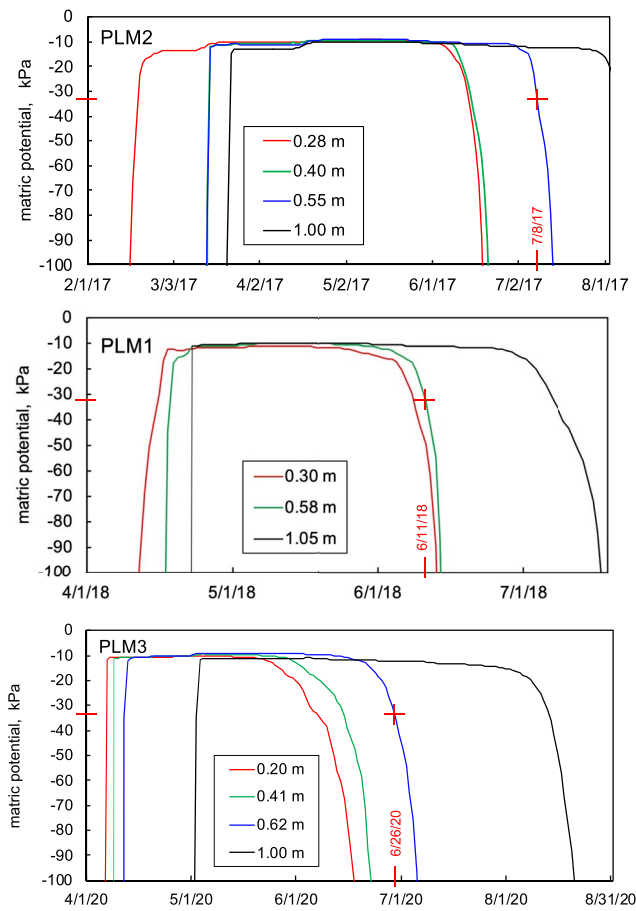


Figure 7. Examples of soil matric potential sensor responses during snowmelt events, illustrating selection of drainage cessation dates when ψ declines below -33 kPa at depths shallower than 1.00 m.

et al., 2021). The decrease in calculated TDN export results from lower overall estimated recharge obtained using the Butte SNOTEL data and improved winter sublimation, greater influence of dilute fluxes via the soil zone during snowmelt, and inclusion of two snow drought years (WY2020 and WY2021) that had low subsurface recharge, hence low TDN export rates.

Subsurface C - Q relations for TDN were generated by plotting correlations between daily values of flow-weighted TDN concentrations (black curve in Figure 6a) and their corresponding total subsurface flow (blue curve in Figure 5b), and presented for each water year in Figure 6c. These results are analogous to more familiar C - Q relations obtained from measurements in rivers (Chanat et al., 2002; Evans & Davies, 1998; Godsey et al., 2009), but reflect predictions of exports along the hillslope transect rather than integrated responses over broader catchments and watersheds. Characteristics of surface water C - Q such as being hysteretic or nonhysteretic, and fitting to the power-law $C = aQ^b$ to describe relations reflecting displacement ($b > 0.1$), chemostasis ($-0.1 \leq b \leq 0.1$), or dilution ($-1 \leq b < -0.1$), are also useful for examining subsurface C - Q behavior. The subsurface C - Q relation for TDN (Figure 6c) are approximately chemostatic, and exhibit weaker clockwise hysteresis for the higher snowmelt years (2017, 2019). The asymmetry in the peaks for total subsurface TDN export rate relative to the peaks in total subsurface flow (Figure 6b) is reflected in clockwise C - Q hysteresis during major snowmelt events (Figure 6c). These patterns are consistent with TDN depletion over the course of subsurface flow during spring snowmelt. Nitrate accounts for most of the TDN in the hillslope subsurface (Wan et al., 2021), and the hysteretic patterns reflecting dissolved N losses may be attributed to denitrification and assimilation (Burns et al., 2019; Ebeling et al., 2021; Ocampo et al., 2006). It should be noted that these processes are also acting in the floodplain to further deplete TDN from pore waters prior to discharge into the river.

3.5. Post-Drainage ET

As noted earlier, cessation of snowmelt drainage was assigned to dates at which $\psi \leq -33$ kPa. MPS-6 sensors are not sensitive to $\psi > -10$ kPa, and cannot record positive pressure potentials. The matric potential sensors embedded in hillslope soils show rapid increases in ψ toward zero during early stages of snowmelt, followed by declining ψ as soils drained. Examples of time trends in ψ during and shortly after snowmelt from the three hillslope stations on different years are shown in Figure 7, with the date at which the sensors shallower than 1.00 m decline back to $\psi \leq -33$ kPa indicated along the time axis. For example, at PLM2, the date for drainage cessation in WY2017 was assigned to July 8, 2017. Collectively, the matric potential sensors showed that snowmelt drainage from soils ceased by June or July of each year. It is worth noting that while sensors at 1.00 m and deeper show less negative ψ , the drainage cessation condition identified by ψ at shallower depths also assures that the hydraulic gradients reflect ET -driven upwardly directed flow.

We now examine soil water contents on dates each year by which soil drainage is insignificant, and compare these amounts with water contents on October 31 in order to determine soil water losses. Example comparisons between such volumetric water content θ_w profiles are shown in Figure 8 for data from 2017 to 2021. Although summer monsoon rain left increased θ_w at the end of October in some of the shallowest soil intervals (e.g., PLM3 2017, and PLM2 2021), net water losses were recorded over all soil profiles, expressed in terms of mm water on each of the graphs. The fact that monsoon rains only increased θ_w and ψ within the shallowest portions of soil profiles indicates that these events do not directly recharge groundwater. The average soil water lost among the three hillslope stations during the monitored post-snowmelt period is indicated above each set of three graphs, and are similar to losses recorded for the other 3 years of this study.

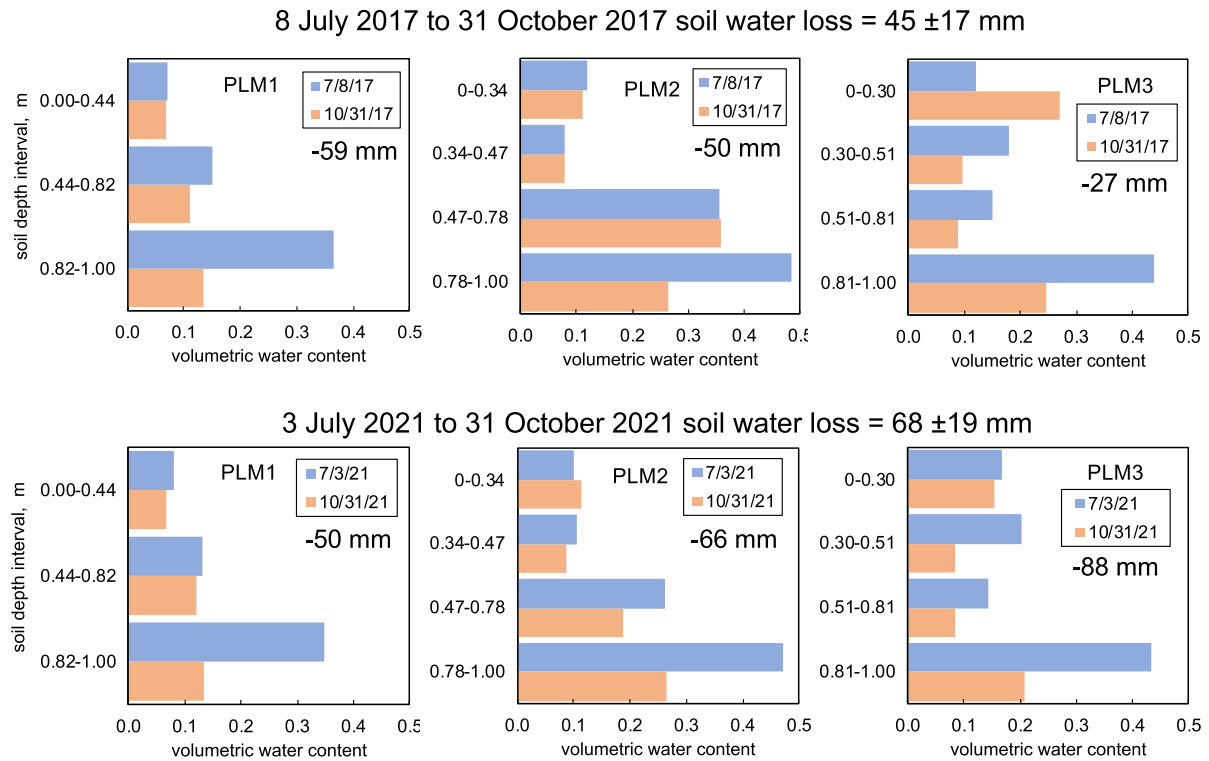


Figure 8. Profiles of volumetric water contents in soils in 2017 and 2021, at cessation of soil drainage (blue), and on October 31. The mm values in each plot indicate soil water losses over the summer to fall intervals.

Soil water losses averaged over the three stations for all 5 years are plotted in Figure 9, along with post-drainage rainfall amounts. Values of soil water mass balance ET obtained from sums of rainfall and soil water loss are compared with $ET(CLM)$ for the same time intervals in Figure 9. The good agreement between water losses determined by soil mass balance and CLM indicate that model predictions during these approximately 4-month periods of summer through fall months were fairly reliable.

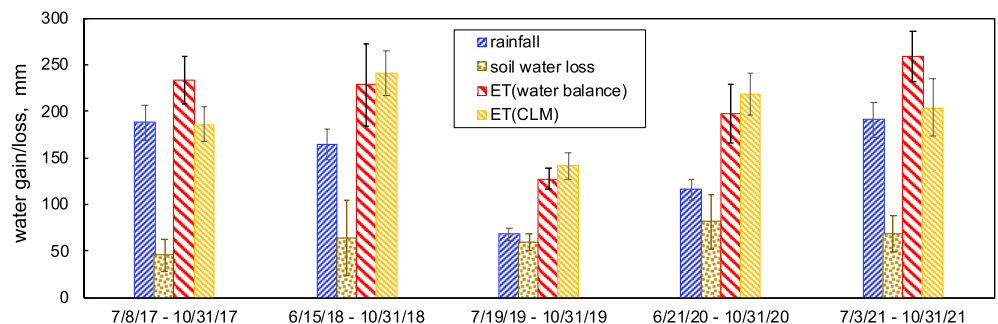


Figure 9. Soil water balance calculations of ET , compared with ET (Community Land Model [CLM]) over summer-fall intervals following cessation of snowmelt drainage. Uncertainties in rainfall and ET (CLM) were estimated as 10% of their respective values, except for the 2021 ET uncertainty which was taken as 15% because its October 2021 ET was estimated from the average of previous Octobers. Uncertainties in soil water losses were assigned to standard errors from values obtained at PLM1, PLM2, and PLM3. Uncertainties in ET (water balance) were estimated as the root mean square uncertainties from summing soil water losses and rainfall.

4. Conclusions

To understand subsurface flow and transport in hillslopes receiving precipitation primarily as snow, annual recharge was used to provide the water mass balance constraint on discharge predicted by the transmissivity feedback model. When measured K profiles were constrained by annual $P-ET$ over only a single year (WY2017), the thickness of the bedrock was adjusted in order for calculated annual subsurface flow to match measured P minus CLM-modeled ET . However, use of the measured K profile in combination with water table elevations measured over all 5 years led to very large discrepancies between predicted subsurface flow and annual $P-ET$. Indeed, the rmsd of 212 mm obtained based on this approach exceeded the expected average recharge (175 mm) for the five years of this study. In view of scale-dependence of K , local measurements are unlikely to properly represent hillslope-scale values, and even the reliability of $P-ET$ was limited because it neglects interannual changes in subsurface water storage.

Based on evidence that local measurements typically underestimate field scale K , the mass balance-constrained transmissivity feedback approach was improved by allowing the three K values (K_{s1} , K_{s2} , K_{wz}) to be optimized in addition to T_{fbr} . Based on evidence that groundwater storage remained higher at the end of water years receiving exceptionally high snowfall, interannual storage variation was represented by allowing snowmelt precipitation that exceeded a threshold level P_{tsp} to contribute to subsurface flow in the subsequent year rather than in the current year. For purposes of estimating subsurface flow, the annual P is replaced by an effective precipitation P_e that reflects interannual transfer of subsurface storage in years when P_{tsp} is exceeded. Thus, five parameters (K_{s1} , K_{s2} , K_{wz} , T_{fbr} , and P_{tsp}) were adjusted to minimize differences between yearly subsurface flow and P_e-ET .

The much greater K values of the soil layers relative to the underlying weathering shale facilitates rapid discharge of snowmelt via temporarily shallow groundwater flow. The resulting hydrograph for subsurface flow during snowmelt rises and falls rapidly, resembling hydrographs of flashy runoff in rivers. Despite the fact that solute concentrations in soil pore waters are generally low, hillslope solute exports during snowmelt in most years largely occur via the soil because of very rapid shallow groundwater flow within the highly transmissive saturated soil. Solute export behavior exemplified here with TDN further support our recent findings that bedrock weathering is the primary source for reactive nitrogen discharged from the hillslope (Wan et al., 2019, 2021). Acceleration of bedrock weathering from consecutive snow drought years is anticipated to result from water table lowering to greater depths, exposing previously permanently reducing shale bedrock to oxygen and driving dissolution of pyrite and carbonate minerals.

Given the importance of ET in determining how much of P becomes subsurface flow, field measurements of ET were included for evaluating model predictions. The soil water balance approach utilizing rainfall data and soil water measurements at three stations long the hillslope yielded measurements of ET from summer through fall that supported CLM calculations. These measurements further support previous conclusions that summer monsoon rainfall does not directly recharge into the hillslope groundwater and underscores the primary role of snowmelt in driving hillslope groundwater flow and solute exports in the study area.

This study showed how hillslope subsurface flow and transport can be quantified based on measurements of water table depths and pore water chemistry, with hydraulic properties constrained by estimates of P and ET . Years with very high recharge from snowmelt raise the water table through the highly transmissive weathering zone and into the even more transmissive soil layers, thereby discharging primarily along these shallow pathways. On the other hand, in snow drought years, low volumes of snowmelt restrict water table rise to remain within the weathering zone, through which most of the snowmelt flow is discharged. Thus, optimizing calculated hydraulic responses to the contrasting discharge dynamics resulting from high snowpack and from snow drought years is essential for improving constraints on estimated K and T . The good agreement (rmsd = 43 mm) between subsurface flow predictions and water mass balance over five water years having large differences in snowpack, and P ranging from 408 to 764 mm, supports this approach for refining transmissivity feedback calculations of hydraulic properties. Moreover, the optimized hydraulic properties were shown to remain well constrained under reasonable variations in assumed P .

After calibration of a hillslope's transmissivity profile with years having widely differing P , future subsurface flow and transport can be estimated based only on measurements of water table depth and pore water chemistry. The ability to represent flow and transport over wide ranges of input from snowmelt is attractive in view of large interannual variations in snowfall and anticipated climate change-driven increased frequency of snow drought

years (Dierauer et al., 2019; Marshall et al., 2019; Shrestha et al., 2021). Given the simplicity of this approach, it can be used for estimating subsurface flow and transport in other catchments instrumented with piezometers and pore water samplers, when measurements or reasonable estimates of P and ET are available.

Data Availability Statement

Data (Tokunaga et al., 2022) used in this study are deposited in the U.S. DOE Environmental Systems Science Data Infrastructure for a Virtual Ecosystem (ESS-DIVE).

Acknowledgments

This work was conducted as part of the Watershed Function Scientific Focus Area at Lawrence Berkeley National Laboratory and was supported by the U.S. Department of Energy (DOE) Subsurface Biogeochemical Research Program, DOE Office of Science, Office of Biological and Environmental Research, under Contract Number DE-AC02-05CH11231. TKT gratefully acknowledges the late Lawrence J. Waldron (April 17, 1925–July 7, 2022), University of California, Berkeley, for mentoring on the soil physics and hydrology principles that were essential for this study. The authors thank the reviewers, Associate Editor, and Editor Peter Troch for helpful comments on earlier versions of this manuscript.

References

- Alvarez-Garretón, C., Boisier, J. P., Garreaud, R., Seibert, J., & Vis, M. (2021). Progressive water deficits during multiyear droughts in basins with long hydrological memory in Chile. *Hydrology and Earth System Sciences*, 25(1), 429–446. <https://doi.org/10.5194/hess-25-429-2021>
- Ameli, A. A., Beven, K., Erlandsson, M., Creed, I. F., McDonnell, J. J., & Bishop, K. (2017). Primary weathering rates, water transit times, and concentration-discharge relations: A theoretical analysis for the critical zone. *Water Resources Research*, 53(1), 942–960. <https://doi.org/10.1002/2016wr019448>
- Anderson, S. P., & Dietrich, W. E. (2001). Chemical weathering and runoff chemistry in a steep headwater catchment. *Hydrological Processes*, 15(10), 1791–1815. <https://doi.org/10.1002/hyp.240>
- Arnone, E., Noto, L. V., Lepore, C., & Bras, R. L. (2011). Physically-based and distributed approach to analyze rainfall-triggered landslides at watershed scale. *Geomorphology*, 133(3–4), 121–131. <https://doi.org/10.1016/j.geomorph.2011.03.019>
- Assouline, S., & Or, D. (2014). The concept of field capacity revisited: Defining intrinsic static and dynamic criteria for soil internal drainage dynamics. *Water Resources Research*, 50(6), 4787–4802. <https://doi.org/10.1002/2014wr015475>
- Bishop, K., Seibert, J., Koher, S., & Laudon, H. (2004). Resolving the double paradox of rapidly mobilized old water with highly variable responses in runoff chemistry. *Hydrological Processes*, 18(1), 185–189. <https://doi.org/10.1002/hyp.5209>
- Boggs, J. M., & Adams, E. E. (1992). Field-study of dispersion in a heterogeneous aquifer. 4. Investigation of adsorption and sampling bias. *Water Resources Research*, 28(12), 3325–3336. <https://doi.org/10.1029/92wr01759>
- Brantley, S. L., Holleran, M. E., Jin, L. X., & Bazilevskaia, E. (2013). Probing deep weathering in the shale hills critical zone observatory, Pennsylvania (USA): The hypothesis of nested chemical reaction fronts in the subsurface. *Earth Surface Processes and Landforms*, 38(11), 1280–1298. <https://doi.org/10.1002/esp.3415>
- Brooks, E. S., Boll, J., & McDaniel, P. A. (2004). A hillslope-scale experiment to measure lateral saturated hydraulic conductivity. *Water Resources Research*, 40(4). <https://doi.org/10.1029/2003wr002858>
- Burns, D. A., Pellerin, B. A., Miller, M. P., Capel, P. D., Tesoriero, A. J., & Duncan, J. M. (2019). Monitoring the riverine pulse: Applying high-frequency nitrate data to advance integrative understanding of biogeochemical and hydrological processes. *Wiley Interdisciplinary Reviews-Water*, 6(4). <https://doi.org/10.1002/wat2.1348>
- Cayan, D. R. (1996). Interannual climate variability and snowpack in the western United States. *Journal of Climate*, 9(5), 928–948. [https://doi.org/10.1175/1520-0442\(1996\)009<0928:icvasi>2.0.co;2](https://doi.org/10.1175/1520-0442(1996)009<0928:icvasi>2.0.co;2)
- Chanat, J. G., Rice, K. C., & Hornberger, G. M. (2002). Consistency of patterns in concentration-discharge plots. *Water Resources Research*, 38(8). <https://doi.org/10.1029/2001wr000971>
- Childs, E. C. (1971). Drainage of groundwater resting on a sloping bed. *Water Resources Research*, 7(5), 1256–1263. <https://doi.org/10.1029/wr007i005p01256>
- Colman, E. A. (1947). A laboratory procedure for determining the field capacity of soils. *Soil Science*, 63(4), 277–284. <https://doi.org/10.1097/00010694-194704000-00003>
- Denager, T., Looms, M. C., Sonnenborg, T. O., & Jensen, K. H. (2020). Comparison of evapotranspiration estimates using the water balance and the eddy covariance methods. *Vadose Zone Journal*, 19(1), 21. <https://doi.org/10.1002/vzj2.20032>
- Dierauer, J. R., Allen, D. M., & Whitfield, P. H. (2019). Snow drought risk and susceptibility in the western United States and southwestern Canada. *Water Resources Research*, 55(4), 3076–3091. <https://doi.org/10.1029/2018wr023229>
- Di Prima, S., Marrosu, R., Lassabatere, L., Angulo-Jaramillo, R., & Pirastru, M. (2018). In situ characterization of preferential flow by combining plot- and point-scale infiltration experiments on a hillslope. *Journal of Hydrology*, 563, 633–642. <https://doi.org/10.1016/j.jhydrol.2018.06.033>
- Ebeling, P., Kumar, R., Weber, M., Knoll, L., Fleckenstein, J. H., & Musolff, A. (2021). Archetypes and controls of riverine nutrient export across German catchments. *Water Resources Research*, 57(4). <https://doi.org/10.1029/2020wr028134>
- Evans, C., & Davies, T. D. (1998). Causes of concentration/discharge hysteresis and its potential as a tool for analysis of episode hydrochemistry. *Water Resources Research*, 34(1), 129–137. <https://doi.org/10.1029/97wr01881>
- Faticchi, S., & Ivanov, V. Y. (2014). Interannual variability of evapotranspiration and vegetation productivity. *Water Resources Research*, 50(4), 3275–3294. <https://doi.org/10.1002/2013wr015044>
- Freeze, R. A. (1972). Role of subsurface flow in generating surface runoff. 2. Upstream source areas. *Water Resources Research*, 8(5), 1272–1283. <https://doi.org/10.1029/wr008i005p01272>
- Freeze, R. A., & Witherspoon, P. A. (1967). Theoretical analysis of regional groundwater flow. 2. Effect of water-table configuration and subsurface permeability variation. *Water Resources Research*, 3(2), 623–634. <https://doi.org/10.1029/wr003i002p0623>
- Garbrecht, J., Van Liew, M., & Brown, G. O. (2004). Trends in precipitation, streamflow, and evapotranspiration in the great plains of the United States. *Journal of Hydrological Engineering*, 9(5), 360–367. [https://doi.org/10.1061/\(asce\)1084-0699\(2004\)9:5\(360\)](https://doi.org/10.1061/(asce)1084-0699(2004)9:5(360))
- Glaser, B., Jackisch, C., Hopp, L., & Klaus, J. (2019). How meaningful are plot-scale observations and simulations of preferential flow for catchment models? *Vadose Zone Journal*, 18(1), 180146. <https://doi.org/10.2136/vzj2018.08.0146>
- Glaser, B., Klaus, J., Frei, S., Frenntress, J., Pfister, L., & Hopp, L. (2016). On the value of surface saturated area dynamics mapped with thermal infrared imagery for modeling the hillslope-riparian-stream continuum. *Water Resources Research*, 52(10), 8317–8342. <https://doi.org/10.1002/2015wr018414>
- Gleeson, T., & Manning, A. H. (2008). Regional groundwater flow in mountainous terrain: Three-dimensional simulations of topographic and hydrogeologic controls. *Water Resources Research*, 44(10), 16. <https://doi.org/10.1029/2008wr006848>
- Godsey, S. E., Kirchner, J. W., & Clow, D. W. (2009). Concentration-discharge relationships reflect chemostatic characteristics of US catchments. *Hydrological Processes*, 23(13), 1844–1864. <https://doi.org/10.1002/hyp.7315>

- Godt, J. W., Baum, R. L., Savage, W. Z., Salciarini, D., Schulz, W. H., & Harp, E. I. (2008). Transient deterministic shallow landslide modeling: Requirements for susceptibility and hazard assessments in a GIS framework. *Engineering Geology*, *102*(3–4), 214–226. <https://doi.org/10.1016/j.enggeo.2008.03.019>
- Hubbert, M. K. (1940). The theory of ground-water motion. *The Journal of Geology*, *48*(8), 785–944. <https://doi.org/10.1086/624930>
- Huntington, T. G., & Billmire, M. (2014). Trends in precipitation, runoff, and evapotranspiration of rivers draining to the Gulf of Maine in the United States. *Journal of Hydrometeorology*, *15*(2), 726–743. <https://doi.org/10.1175/jhm-d-13-018.1>
- Jencso, K. G., McGlynn, B. L., Gooseff, M. N., Bencala, K. E., & Wondzell, S. M. (2010). Hillslope hydrologic connectivity controls riparian groundwater turnover: Implications of catchment structure for riparian buffering and stream water sources. *Water Resources Research*, *46*, W10524. <https://doi.org/10.1029/2009wr008818>
- Kendall, K. A., Shanley, J. B., & McDonnell, J. J. (1999). A hydrometric and geochemical approach to test the transmissivity feedback hypothesis during snowmelt. *Journal of Hydrology*, *219*(3–4), 188–205. [https://doi.org/10.1016/s0022-1694\(99\)00059-1](https://doi.org/10.1016/s0022-1694(99)00059-1)
- Kuang, X. X., & Jiao, J. J. (2014). An integrated permeability-depth model for Earth's crust. *Geophysical Research Letters*, *41*(21), 7539–7545. <https://doi.org/10.1002/2014gl061999>
- Lute, A. C., & Abatzoglou, J. T. (2014). Role of extreme snowfall events in interannual variability of snowfall accumulation in the western United States. *Water Resources Research*, *50*(4), 2874–2888. <https://doi.org/10.1002/2013wr014465>
- Marshall, A. M., Abatzoglou, J. T., Link, T. E., & Tennant, C. J. (2019). Projected changes in interannual variability of peak snowpack amount and timing in the western United States. *Geophysical Research Letters*, *46*(15), 8882–8892. <https://doi.org/10.1029/2019gl083770>
- Maule, C. P., & Chanasyk, D. S. (1987). A comparison of two methods for determining the evapotranspiration and drainage components of the soil water balance. *Canadian Journal of Soil Science*, *67*(1), 43–54. <https://doi.org/10.4141/cjss87-004>
- McGuire, K. J., & McDonnell, J. J. (2010). Hydrological connectivity of hillslopes and streams: Characteristic time scales and nonlinearities. *Water Resources Research*, *46*, W10543. <https://doi.org/10.1029/2010wr009341>
- Michalzik, B., Kalbitz, K., Park, J. H., Solinger, S., & Matzner, E. (2001). Fluxes and concentrations of dissolved organic carbon and nitrogen — A synthesis for temperate forests. *Biogeochemistry*, *52*(2), 173–205. <https://doi.org/10.1023/a:1006441620810>
- Miller, M. P., Susong, D. D., Shope, C. L., Heilweil, V. M., & Stolp, B. J. (2014). Continuous estimation of baseflow in snowmelt-dominated streams and rivers in the upper Colorado River Basin: A chemical hydrograph separation approach. *Water Resources Research*, *50*(8), 6986–6999. <https://doi.org/10.1002/2013wr014939>
- Niu, J., Shen, C. P., Chambers, J. Q., Melack, J. M., & Riley, W. J. (2017). Interannual variation in hydrologic budgets in an Amazonian watershed with a coupled subsurface-land surface process model. *Journal of Hydrometeorology*, *18*(9), 2597–2617. <https://doi.org/10.1175/jhm-d-17-0108.1>
- Ocampo, C. J., Oldham, C. E., Sivapalan, M., & Turner, J. V. (2006). Hydrological versus biogeochemical controls on catchment nitrate export: A test of the flushing mechanism. *Hydrological Processes*, *20*(20), 4269–4286. <https://doi.org/10.1002/hyp.6311>
- Oleson, K. W., Lawrence, D. M., Bonan, G. B., Drewniak, B., Huang, M., Koven, C. D., et al. (2013). Technical description of version 4.5 of the community land model (CLM). Retrieved from boulder, Colorado.
- Penna, D., Van Meerveld, H. J., Oliviero, O., Zuecco, G., Assendelft, R. S., Dalla Fontana, G., & Borga, M. (2015). Seasonal changes in runoff generation in a small forested mountain catchment. *Hydrological Processes*, *29*(8), 2027–2042.
- Pinder, G. F., & Jones, J. F. (1969). Determination of the ground-water component of peak discharge from chemistry of total runoff. *Water Resources Research*, *5*(2), 438–445. <https://doi.org/10.1029/wr005i002p00438>
- Rana, G., & Katerji, N. (2000). Measurement and estimation of actual evapotranspiration in the field under mediterranean climate: A review. *European Journal of Agronomy*, *13*(2–3), 125–153. [https://doi.org/10.1016/s1161-0301\(00\)00070-8](https://doi.org/10.1016/s1161-0301(00)00070-8)
- Rice, J. S., & Emanuel, R. E. (2019). Ecohydrology of interannual changes in watershed storage. *Water Resources Research*, *55*(10), 8238–8251. <https://doi.org/10.1029/2019wr025164>
- Rodhe, A. (1989). On the generation of stream runoff in till soils. *Nordic Hydrology*, *20*(1), 1–8. <https://doi.org/10.2166/nh.1989.0001>
- Rogora, M., Somaschini, L., Marchetto, A., Mosello, R., Tartari, G. A., & Paro, L. (2020). Decadal trends in water chemistry of Alpine lakes in calcareous catchments driven by climate change. *Science of the Total Environment*, *708*, 14. <https://doi.org/10.1016/j.scitotenv.2019.135180>
- Rosenbaum, U., Huisman, J. A., Weuthen, A., Vereecken, H., & Bogaen, H. R. (2010). Sensor-to-sensor variability of the ECH2O EC-5, TE, and 5TE sensors in dielectric liquids. *Vadose Zone Journal*, *9*(1), 181–186. <https://doi.org/10.2136/vzj2009.0036>
- Sanford, W. E. (2017). Estimating regional-scale permeability-depth relations in a fractured-rock terrain using groundwater-flow model calibration. *Hydrogeology Journal*, *25*(2), 405–419. <https://doi.org/10.1007/s10040-016-1483-y>
- Saxton, K. E., Rawls, W. J., Romberger, J. S., & Papendick, R. I. (1986). Estimating generalized soil-water characteristics from texture. *Soil Science Society of America Journal*, *50*(4), 1031–1036. <https://doi.org/10.2136/sssaj1986.03615995005000040039x>
- Sexstone, G. A., Clow, D. W., Stannard, D. I., & Fassnacht, S. R. (2016). Comparison of methods for quantifying surface sublimation over seasonally snow-covered terrain. *Hydrological Processes*, *30*(19), 3373–3389. <https://doi.org/10.1002/hyp.10864>
- Shrestha, R. R., Bonsal, B. R., Bonnyman, J. M., Cannon, A. J., & Najafi, M. R. (2021). Heterogeneous snowpack response and snow drought occurrence across river basins of northwestern North America under 1.0°C to 4.0°C global warming. *Climatic Change*, *164*(3–4). <https://doi.org/10.1007/s10584-021-02968-7>
- Spencer, S. A., Anderson, A. E., Silins, U., & Collins, A. L. (2021). Hillslope and groundwater contributions to streamflow in a rocky mountain watershed underlain by glacial till and fractured sedimentary bedrock. *Hydrology and Earth System Sciences*, *25*(1), 237–255. <https://doi.org/10.5194/hess-25-237-2021>
- Todd, A. S., Manning, A. H., Verplanck, P. L., Crouch, C., McKnight, D. M., & Dunham, R. (2012). Climate-change-driven deterioration of water quality in a mineralized watershed. *Environmental Science & Technology*, *46*(17), 9324–9332. <https://doi.org/10.1021/es3020056>
- Tokunaga, T. (1992). The pressure response of the soil water sampler and possibilities for simultaneous soil solution sampling and tensiometry. *Soil Science*, *154*(3), 171–183. <https://doi.org/10.1097/00010694-199209000-00001>
- Tokunaga, T. K., Tran, A. P., Wan, J., Dong, W., Newman, A. W., Beutler, C. A., et al. (2022). Data used in manuscript "quantifying subsurface flow and solute transport in a snowmelt-recharged hillslope with multiyear water balance". *Water Resources Research*. <https://doi.org/10.15485/1874376>
- Tokunaga, T. K., Wan, J., Williams, K. H., Brown, W., Henderson, A., Kim, Y., et al. (2019). Depth- and time-resolved distributions of snowmelt-driven hillslope subsurface flow and transport and their contributions to surface waters. *Water Resources Research*, *55*, 9474–9499. <https://doi.org/10.1029/2019wr025093>
- Toth, J. (1963). A theoretical analysis of groundwater flow in small drainage basins. *Journal of Geophysical Research*, *68*(16), 4795–4812. <https://doi.org/10.1029/jz068i016p04795>

- Toure, A. M., Luojus, K., Rodell, M., Beaudoin, H., & Getirana, A. (2018). Evaluation of simulated snow and snowmelt timing in the community land model using satellite-based products and streamflow observations. *Journal of Advances in Modeling Earth Systems*, *10*(11), 2933–2951. <https://doi.org/10.1029/2018ms001389>
- Toure, A. M., Rodell, M., Yang, Z. L., Beaudoin, H., Kim, E., Zhang, Y. F., & Kwon, Y. W. (2016). Evaluation of the snow simulations from the community land model, version 4 (CLM4). *Journal of Hydrometeorology*, *17*(1), 153–170. <https://doi.org/10.1175/jhm-d-14-0165.1>
- Tran, A. P., Rungee, J., Faybishenko, B., Dafflon, B., & Hubbard, S. S. (2019). Assessment of spatiotemporal variability of evapotranspiration and its governing factors in a mountainous watershed. *Water*, *11*, 243. <https://doi.org/10.3390/w11020243>
- Uchida, T., Kosugi, K., & Mizuyama, T. (2001). Effects of pipeflow on hydrological process and its relation to landslide: A review of pipeflow studies in forested headwater catchments. *Hydrological Processes*, *15*(11), 2151–2174. <https://doi.org/10.1002/hyp.281>
- Uchida, T., Meerveld, I. T., & McDonnell, J. J. (2005). The role of lateral pipe flow in hillslope runoff response: An intercomparison of non-linear hillslope response. *Journal of Hydrology*, *311*(1–4), 117–133. <https://doi.org/10.1016/j.jhydrol.2005.01.012>
- USDA, N. (2021). Colorado SNOTEL site butte (380). Retrieved from <https://wcc.sc.egov.usda.gov/nwcc/site?sitenum=380>
- Versteeg, R., & Williams, K. H. (2021). LBNL SFA 2.0 data management site. Retrieved from https://lbnlsfa.paf.subsurfaceinsights.com/login/?redir=%2Fdatadownload%2F%26show_redir_msg=1
- Wan, J. M., Tokunaga, T. K., Brown, W., Newman, A. W., Dong, W. M., Bill, M., et al. (2021). Bedrock weathering contributes to subsurface reactive nitrogen and nitrous oxide emissions. *Nature Geoscience*, *14*(4), 217–224. <https://doi.org/10.1038/s41561-021-00717-0>
- Wan, J. M., Tokunaga, T. K., Williams, K. H., Dong, W. M., Brown, W., Henderson, A. N., et al. (2019). Predicting sedimentary bedrock subsurface weathering fronts and weathering rates. *Scientific Reports*, *9*. <https://doi.org/10.1038/s41598-019-53205-2>
- Wang, D. B. (2012). Evaluating interannual water storage changes at watersheds in Illinois based on long-term soil moisture and groundwater level data. *Water Resources Research*, *48*(3), 12. <https://doi.org/10.1029/2011wr010759>
- Weihermuller, L., Kasteel, R., & Vereecken, H. (2006). Soil heterogeneity effects on solute breakthrough sampled with suction cups: Numerical simulations. *Vadose Zone Journal*, *5*(3), 886–893. <https://doi.org/10.2136/vzj2005.0105>
- Weiler, M., McDonnell, J. J., Tromp-van Meerveld, I., & Uchida, T. (2005). Subsurface stormflow. In M. G. Anderson (Ed.) *Encyclopedia of Hydrological Sciences* (Vol. 112, pp. 14). John Wiley & Sons, Ltd. <https://doi.org/10.1002/0470848944.hsa119>
- Wilson, G. V., Rigby, J. R., Ursic, M., & Dabney, S. M. (2016). Soil pipe flow tracer experiments: 1. Connectivity and transport characteristics. *Hydrological Processes*, *30*(8), 1265–1279. <https://doi.org/10.1002/hyp.10713>
- Winnick, M. J., Carroll, R. W. H., Williams, K. H., Maxwell, R. M., Dong, W. M., & Maher, K. (2017). Snowmelt controls on concentration-discharge relationships and the balance of oxidative and acid-base weathering fluxes in an alpine catchment, East River, Colorado. *Water Resources Research*, *53*(3), 2507–2523. <https://doi.org/10.1002/2016wr019724>
- Woodhouse, C. A., & Pederson, G. T. (2018). Investigating runoff efficiency in upper Colorado River streamflow over past centuries. *Water Resources Research*, *54*(1), 286–300. <https://doi.org/10.1002/2017wr021663>
- Xiao, M., Udall, B., & Lettenmaier, D. P. (2018). On the causes of declining Colorado River streamflows. *Water Resources Research*, *54*(9), 6739–6756. <https://doi.org/10.1029/2018wr023153>

Erratum

In the originally published version of this article, the second author's first name was incorrectly spelled as Ahn, and his affiliation was incorrectly listed as Water Research Institute. The spelling has been corrected to Anh, and the affiliation has been corrected to Water Resources Institute. Also, there were five errors in section 3.1 which involved the insertion of an extraneous “1” in the exponents. 10^{-15} should read 10^{-5} . 10^{-14} should read 10^{-4} (two instances). 10^{-16} should read 10^{-6} . These errors have corrected, and this may be considered the authoritative version of record.